Chemical pressure and hidden one-dimensional behavior in rare-earth tri-telluride charge-density wave compounds

A. Sacchetti and L. Degiorgi
Laboratorium für Festkörperphysik, ETH - Zürich, CH-8093 Zürich, Switzerland

T. Giamarchi
DPMC-MaNEP, University of Geneva, 24, quai Ernest-Ansermet, CH-1211 Geneva 4, Switzerland

N. Ru and I. R. Fisher
Geballe Laboratory for Advanced Materials and Department of Applied Physics, Stanford University, Stanford, California 94305-4045, USA

(Received 19 June 2006; published 26 September 2006)

We report on the first optical measurements of the rare-earth tri-telluride charge-density wave systems. Our data, collected over an extremely broad spectral range, allow us to observe both the Drude component and the single-particle peak, ascribed to the contributions due to the free charge carriers and to the charge-density wave gap excitation, respectively. The data analysis displays a diminishing impact of the charge-density wave condensate on the electronic properties with decreasing lattice constant across the rare-earth series. We propose a possible mechanism describing this behavior and we suggest the presence of a one-dimensional character in these two-dimensional compounds. We also envisage that interactions and umklapp processes might play a relevant role in the formation of the charge-density wave state in these compounds.

DOI: 10.1103/PhysRevB.74.125115 PACS number(s): 71.45.Lr, 78.20.−e

I. INTRODUCTION

Low dimensionality is an important issue in solid state physics,[1] owing to the general tendency of low-dimensional systems to form charge- and spin-density wave (CDW and SDW) states.[2,3] CDW and SDW phases are broken symmetry ground states driven by the electron-phonon and electron-electron interactions, respectively. These phases, from the electronic point of view, are induced by nesting of the Fermi surface (FS).[2] Besides the single particle gap excitation, the density wave states are then characterized by the formation of the collective CDW or SDW condensate.[2] Density waves have been observed in several materials such as linear-chain organic and inorganic compounds.[2] Strong interest in low-dimensional systems has also been brought about by the considerable deviations of their normal state properties from those of a Fermi liquid.[4–7] In one dimension, the Tomonaga-Luttinger-liquid or Luther-Emery scenarios, implying phenomena such as spin-charge separation and non-universal power-law behavior of the spectral functions, are most suitable.[7] In several cases, characteristic and peculiar power-law behaviors were indeed observed in the spectroscopic (optical and photoemission) properties of various quasi one-dimensional materials.[5–7] It is worth noting that, although the theory of density waves is well established in the one-dimensional (1D) case,[2] little is known about the two-dimensional (2D) case.

Another class of compounds, which recently gained importance in the study of density waves, are the rare-earth tri-tellurides $R\mathrm{Te}_3$ [R is La–Tm, excepting Eu (Ref. 8)]. These systems exhibit an incommensurate CDW, stable across the available rare-earth series.[9] All these compounds have the same average crystal structure (belonging to the *Cmcm* space group[10]) made up of square planar Te sheets[11] and insulating corrugated RTe layers which act as charge reservoirs for the Te planes. The lattice constant decreases on going from R as La to R as Tm,[12] i.e., by decreasing the ionic radius of the rare-earth atom. Therefore, the study of these compounds allows one to investigate the CDW state as a function of the unit-cell volume and in particular of the in-plane lattice constant a, which is directly related to the Te-Te distance in the Te layers.

Metallic conduction occurs along the Te sheets leading to highly anisotropic transport properties. For instance, the ratio between the in- and out-of-plane conductivity can be as high as 3000.[8] The rare-earth atom is trivalent for all members of the series[8] and thus the electronic structure is quite similar in all of them. Band structure calculations[9,13,14] reveal that the electronic bands at the Fermi level derive from the Te p_x and p_y in-plane orbitals, leading to a very simple FS, a large part of which is nested by a single wave vector $\vec{q}=(0,x)$, $x \simeq 0.29a^*$ ($a^*=2\pi/a$) in the base plane of the reciprocal lattice.[14] This nesting appears to be the driving mechanism for the CDW instability.[15,16]

The compounds are characterized by an unusually large CDW gap, which was observed by angle resolved photoemission spectroscopy (ARPES) measurements. The CDW gap ranges between 200 and 400 meV, depending on the rare earth.[15–19] Consistent with these large gap values, $R\mathrm{Te}_3$ compounds are well within the CDW state already at room temperature and the CDW transition temperature (T_{CDW}) is believed to be even higher than the melting point.[17] Owing to the 2D character of these compounds, the gap is not isotropic and shows a wave-vector dependence.[16,17] In particular, since the vector $\vec{q}$ does not nest the whole FS, there are parts of it which are not gapped. Therefore, the CDW state coexists with the metallic phase due to the free charge carriers in the ungapped regions of the FS. The study of these compounds

 ©2006 The American Physical Society

could give, in principle, an important insight into the interplay between the metallic state and the broken-symmetry CDW phase. Furthermore, the presence of a single nesting vector defines a preferred crystallographic direction for the development of the CDW state, and leads to features typical of a 1D system, despite the 2D character of these compounds.

Besides to the prototype 1D systems,[2] optical spectroscopy was already successfully applied to the study of 2D chalcogenides such as $NbSe_2$ and $TaSe_2$, where anomalous behavior of the carriers' scattering rate was observed in the CDW phase,[20,21] as well as $NbSe_3$ and $TaSe_3$, where a polaronic scenario for the CDW was proposed.[22,23] Here we describe the first comprehensive optical study on RTe_3. Optical spectroscopy is in general an ideal tool to study CDW systems,[2] since it is able to reveal the opening of the CDW gap in the charge excitation spectrum. The optical signature of the CDW phase is in fact a finite-frequency peak, ascribed to the transition from the CDW condensate to a single particle (SP) state.[24] Moreover, because of the imperfect nesting, as typical for quasi 2D systems such as RTe_3, the optical technique also reveals the free-carriers contribution in terms of a Drude peak.

II. EXPERIMENT AND RESULTS

We report on optical reflectivity measurements carried out on RTe_3 single crystals for representative members across the rare-earth series R as La, Ce, Nd, Sm, Gd, Tb, and Dy. Single crystal samples were grown by slow cooling a binary melt, as described elsewhere.[25] Platelike crystals up to several mm in diameter were removed from the melt by decanting in a centrifuge. The crystals could be readily cleaved between Te layers to reveal clean surfaces for the reflectivity measurements. Exploiting several spectrometers and interferometers, the optical reflectivity $R(\omega)$ was measured for all samples from the far-infrared (6 meV) up to the ultraviolet (12 eV) spectral range, with light polarized parallel to the Te planes. Details pertaining to the experiments can be found elsewhere.[26,27]

Figure 1 displays the overall $R(\omega)$ spectra for selected members across the rare-earth series. Consistently with the large gap values, no temperature dependence of the spectrum was observed between 2 K and 300 K. As expected from the presence of ungapped regions of the FS, all samples exhibit a metallic $R(\omega)$, tending to total reflection at zero frequency [i.e., $R(\omega)\rightarrow 1$, for $\omega\rightarrow 0$], and the appearance of a plasma edge around 10 000 cm^{-1}. Above the plasma edge, several spectral features are also observed. At lower frequency a bump is apparent in $R(\omega)$ of all samples (see inset of Fig. 1). This feature is more evident in $LaTe_3$ but it becomes progressively less pronounced and shifts to lower frequency on going from $LaTe_3$ to $DyTe_3$, i.e., on decreasing the in-plane lattice constant a.

The large explored spectral range allows us to perform reliable Kramers-Kronig (KK) transformations. To this end, $R(\omega)$ was extended towards zero frequency (i.e., $\omega\rightarrow 0$) with the Hagen-Rubens extrapolation $[R(\omega)=1-2\sqrt{\omega/\sigma_{dc}}]$ and with standard power-law extrapolations at high frequencies.[26] The dc conductivity values employed in the Hagen-Rubens extension of $R(\omega)$ are consistent with transport measurements.[25,28] The KK transformations allow us to extract the real part $\sigma_1(\omega)$ of the optical conductivity, displayed in Fig. 2.

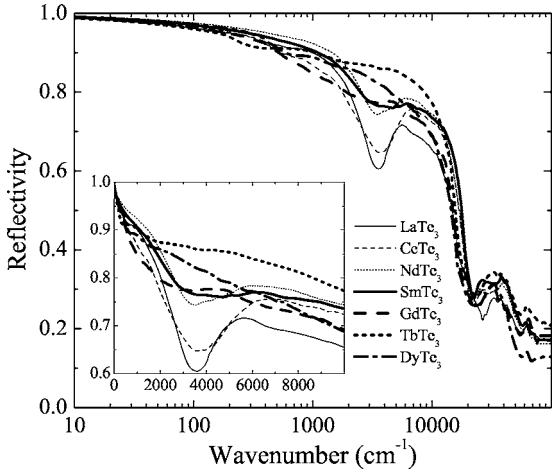

FIG. 1. $R(\omega)$ at room temperature of RTe_3 (R is La, Ce, Nd, Sm, Gd, Tb, and Dy). The inset shows a blow up of the $R(\omega)$ in the energy range between 0 and 10 000 cm^{-1}.

III. DISCUSSION

All $\sigma_1(\omega)$ spectra in Fig. 2 are characterized by the presence of two main features, namely a Drude peak, revealing metallic conduction due to the free charge carriers, and a second midinfrared peak centered at finite frequency (arrows in Fig. 2), corresponding to the bump observed in $R(\omega)$ (Fig. 1). The depletion in the $\sigma_1(\omega)$ spectrum between these two features will be later identified with the CDW gap. Higher energy excitations, corresponding to the spectral features ob-

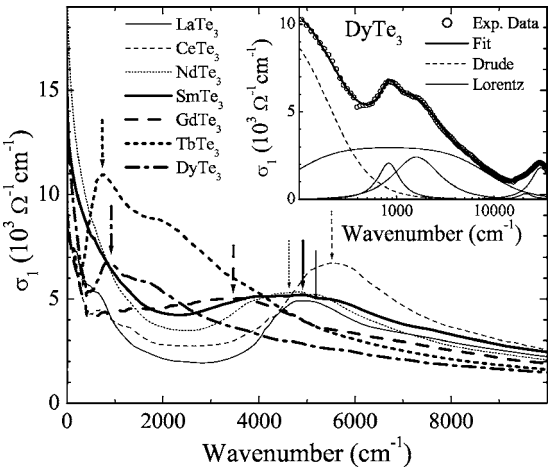

FIG. 2. Room temperature $\sigma_1(\omega)$ of RTe_3 (R is La, Ce, Nd, Sm, Gd, Tb, and Dy). Arrows mark the position of the SP peak for each compound (see text). Inset: Drude-Lorentz fit for $DyTe_3$, showing the experimental data, the fitted curve, and the Drude and the Lorentz components.

served in $R(\omega)$ above the plasma edge, are also present in σ_1 (not shown in the figure) and they are ascribed to electronic interband transitions. The frequencies of these excitations are compatible with the predictions from band-structure calculations,[13,14] taking into account the band energies at the Γ point. On the other hand, these band-structure calculations do not reveal any electronic transition below 1 eV for the undistorted structure (i.e., in the normal state). It is thus natural to identify the depletion in the $\sigma_1(\omega)$ spectrum between the Drude and the midinfrared peaks with the CDW gap. Therefore, the midinfrared peak is ascribed to the charge excitation across the CDW gap into a single-particle (SP) state. In the following we will refer to this peak as the SP peak.

Interestingly, our data show a clear redshift of the SP peak from $LaTe_3$ to $DyTe_3$. This effect can be observed directly from the $\sigma_1(\omega)$ spectra (arrows in Fig. 2) or, to a smaller extent, from $R(\omega)$ (inset of Fig. 1). In order to obtain more quantitative information, a fit procedure, exploiting the phenomenological Drude-Lorentz model, was carried out on all spectra. It consists in reproducing the dielectric function by the following expression (Refs. 26 and 27):

$$\tilde{\epsilon}(\omega) = \epsilon_1(\omega) + i\epsilon_2(\omega) = \epsilon_\infty - \frac{\omega_P^2}{\omega^2 + i\omega\gamma_D} + \sum_j \frac{S_j^2}{\omega^2 - \omega_j^2 - i\omega\gamma_j}, \quad (1)$$

where ϵ_∞ is the optical dielectric constant, ω_P and γ_D are the plasma frequency and the width of the Drude peak, whereas ω_j, γ_j, and S_j^2 are the center-peak frequency, the width, and the mode strength for the jth Lorentz harmonic oscillator (HO), respectively. $\sigma_1(\omega)$ is then obtained from $\sigma_1(\omega) = \omega\epsilon_2(\omega)/4\pi$.

The fit of all spectra were extended up to 40 000 cm^{-1}. Besides the Drude contribution, five Lorentz HO's for each compound are required to fit the finite-frequency features. This is explicitly shown in the inset of Fig. 2 for $DyTe_3$, where the single fit components are displayed. The three low frequency oscillators allow one to reproduce the rather broad absorption, ascribed to the SP peak. This choice is motivated by the fact that, for all samples, the SP peak cannot be fitted with a single Lorentzian oscillator. There is indeed the presence of low- and high-frequency shoulders, each described by a Lorentz HO, which overlap to a background defined by a broad HO. In $LaTe_3$ and $CeTe_3$ the shoulder at the low-frequency side of the SP peak almost merges with the high-frequency tail of the Drude component. Therefore, the SP peak in each compound can be thought as composed by the superposition of several excitations, which mimic the continuous distribution of gap values, as observed by ARPES.[15–19] The remaining two high frequency HO's account for the optical (electronic interband) transitions.

There are several interesting parameters, which can be extracted from the fit. First of all, the plasma frequency ω_P, the square of which represents the total spectral weight of the Drude peak. The larger ω_P is, the higher is the metallic degree of the system. It is also worth it to recall that $\omega_P^2 \propto n/m^*$, where n is the charge-carriers' density and m^* is the carriers' effective mass. The obtained values of ω_P are plotted in Fig. 3(a), as a function of the lattice constant a.[12] An increase of ω_P going from $LaTe_3$ to $DyTe_3$ is well evident.

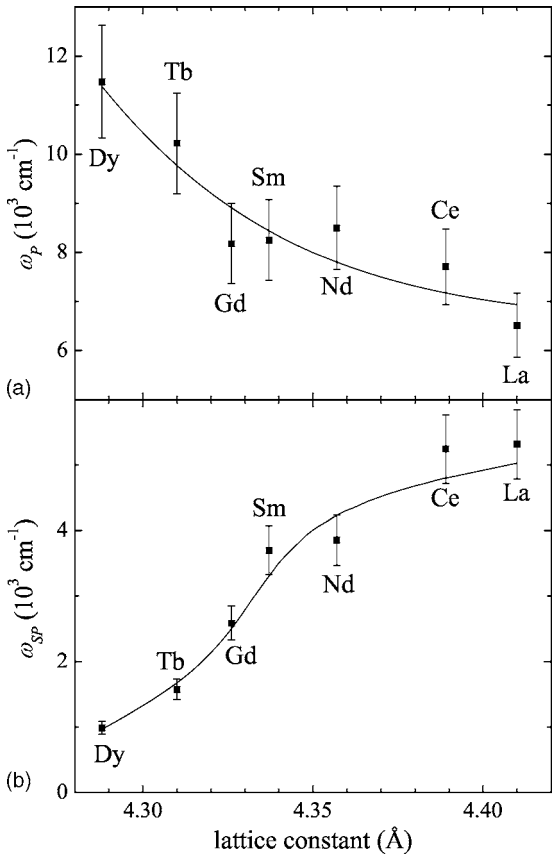

FIG. 3. Plasma frequency (a) and single-particle peak frequency (b) as a function of the in-plane lattice constant (Ref. 12). The rare-earth atom for each compound is shown in the plot. The solid lines are guides to eyes.

As to the SP peak, since it is composed by three Lorentz HO's, we define the averaged quantity ω_{SP},

$$\omega_{SP} = \frac{\sum_{j=1}^{3} \omega_j S_j^2}{\sum_{j=1}^{3} S_j^2}, \quad (2)$$

which represents the center of mass of the SP excitation and thus provides an optical estimate for the CDW gap. In Fig. 3(b), ω_{SP} is plotted as a function of a.[12] The decrease of ω_{SP} (thus of the average gap value) is well evident on going from $LaTe_3$ to $DyTe_3$, oppositely to the observed increase of ω_P [thus of the Drude spectral weight, Fig. 3(a)]. Another interesting quantity associated to the SP-peak is the total spectral weight S_{SP}^2 of the (broad) SP excitation, which is defined as

$$S_{SP}^2 = \sum_{j=1}^{3} S_j^2. \quad (3)$$

At this point we are then equipped for a thorough discussion of our findings. Before addressing in detail the evolution of the electronic properties across the rare-earth series, we first focus our attention on the relationship between the

TABLE I. Effective mass m_{NS} and carriers' density n_{NS} in the normal state and effective mass m_{CDW} and carriers' density n_{CDW} in the CDW state for all samples. Carriers' densities and effective masses are given in carriers per cell and m_e units, respectively. The last column reports the ratio Φ between the Drude spectral weights (see text) in the CDW and normal state. Experimental uncertainties in the last digits are given in brackets.

Sample	m_{NS}	n_{NS}	m_{CDW}	n_{CDW}	$\Phi=\omega_P^2/S_{NS}^2$
$LaTe_3$	1.1(1)	12(2)	0.56(6)	0.13(1)	0.021(4)
$CeTe_3$	1.1(1)	15(3)	0.56(6)	0.18(2)	0.024(5)
$NdTe_3$	1.2(1)	14(3)	0.59(6)	0.23(2)	0.032(6)
$SmTe_3$	1.2(1)	17(4)	0.59(6)	0.22(2)	0.025(5)
$GdTe_3$	1.2(1)	13(3)	0.59(6)	0.22(2)	0.032(6)
$TbTe_3$	1.2(1)	17(4)	0.60(6)	0.34(3)	0.041(8)
$DyTe_3$	1.2(1)	13(3)	0.60(6)	0.43(4)	0.065(13)

CDW and the normal state (NS) properties for each compound. Although the high-temperature NS cannot be studied experimentally since T_{CDW} is anticipated to be above the melting point of the material, we can nevertheless draw some predictions by exploiting our data and the band-structure calculations.[13,14] The Te p_x and p_y orbitals have a strong 2D character (i.e., they have a negligible dispersion along the direction orthogonal to the Te layers). These bands are well approximated by a tight-binding model[15] in which, taking into account the stoichiometry, the Fermi level lies above half-filling (i.e., at 3.25 eV below the top of the bands),[29] indicating that charge carriers are holelike. Considering a parabolic expansion of the 2D bands around their maximum, the Fermi energy E_F=3.25 eV, within a 2D free-holes model, is then related to the effective mass m_{NS} by

$$E_F = \frac{\pi\hbar^2 n_{2D}}{m_{NS}}, \tag{4}$$

where n_{2D} is the 2D hole density in NS. This latter quantity is determined by assuming 1.5 holes for each tellurium atom within the Te layers and 2 Te atoms for each square unit within the 2D layers (i.e., $n_{2D}=3/a^2$). From n_{2D} and E_F, we achieve m_{NS} for each sample by exploiting Eq. (4). The m_{NS} values are reported in Table I.

The m_{NS} values allow us to check our data in a self-consistent manner. If we assume the conservation of the spectral weight between the CDW and the normal state, and that there will be no SP peak in the (hypothetical) NS, the Drude contribution in NS would then have a total spectral weight given by $S_{NS}^2=\omega_P^2+S_{SP}^2$ (Fig. 3). Therefore, from $S_{NS}^2 \sim n_{NS}/m_{NS}$ we can estimate the three-dimensional carriers density n_{NS} in NS, as reported in Table I for each compound. This quantity can be compared with the carriers' density n_{ch} obtained from the chemical counting. Since the 3D unit cell contains four Te layers (i.e., eight Te atoms) with 1.5 holes for each Te atom, we obtain n_{ch}=12 holes/cell. The fair agreement (at least within the experimental uncertainties) between n_{NS} and n_{ch} is well evident in Table I. This finding makes us confident about the reliability of our analysis.

We now consider the free charge carriers surviving in the CDW state. We can estimate their effective mass m_{CDW} from the existing specific heat data on $LaTe_3$. The Sommerfeld γ value of the linear term in the specific heat is γ=0.0011 J mol^{-1} K^{-2} for $LaTe_3$.[25,29] We assume a 2D free-holes scenario for the ungapped carriers also in the CDW phase. Within this approach, γ and m_{CDW} are related by

$$\gamma = \frac{\pi k_B^2 m_{CDW} a^2}{3\hbar^2}. \tag{5}$$

Since γ is difficult to extract from heat capacity measurements for the magnetic members of the rare-earth series, we use the value of $LaTe_3$ for all samples. Bearing in mind the small chemical and structural changes occurring across the rare-earth series, this assumption appears reasonable. Therefore, we can estimate m_{CDW} from Eq. (5) for all samples, as reported in Table I. It turns out that the free-carriers' mass decreases by a factor 2 on entering the CDW state. This finding can be explained by noting again that in RTe_3 the relevant electronic states correspond to the two orthogonal bands deriving from the Te p_x and p_y orbitals. The band structure, while nearly 2D, is anisotropic in the plane. Therefore, m_{NS} and m_{CDW} should be considered as parameters describing the average curvature of the free charge carriers bands in the normal and CDW state, respectively. In this respect, our estimates of the effective masses represent a harmonic average of the mass per carrier, i.e., $1/m_{NS}=1/n_{NS}\Sigma_i 1/m_i$ and $1/m_{CDW}=1/n_{CDW}\Sigma_i 1/m_i$, where the two sums run over the ungapped states in the normal and CDW phases, respectively. The difference in the m_{NS} and m_{CDW} values thus indicates that in the CDW phase the average band curvature is larger than in NS. Consequently, the CDW mainly gaps "heavy" carriers (i.e., those belonging to states with small band curvature). The remaining ungapped carriers thus occupy states with a larger band curvature, resulting in smaller effective mass. Since states with small band curvature are flatter (i.e., they have a smaller dispersion) than those with large band curvature, one can expect the former to give a larger contribution to the density of states than the latter. Therefore, it is not at all surprising that the CDW tends to gap states with the small band curvature. This way there are more states which can be gapped and the CDW energy gain is larger.

The knowledge of m_{CDW} and ω_P allows us to determine the density n_{CDW} of the ungapped carriers in the CDW phase. The n_{CDW} values for each sample are reported in Table I. The large difference between n_{NS} and n_{CDW} and consequently the dramatic reduction of the number of ungapped charge carriers indicate the strong effect of the CDW formation; a large part of the charge carriers takes part in the formation of the CDW condensate. That a significant part of the FS is gapped in the CDW phase, is confirmed by ARPES data from which the fraction of the ungapped FS can be estimated to be 10–20 %.[15–18]

In this respect, the quantity $\Phi=\omega_P^2/(\omega_P^2+S_{SP}^2)$ is of interest, since it represents the ratio between the spectral weight

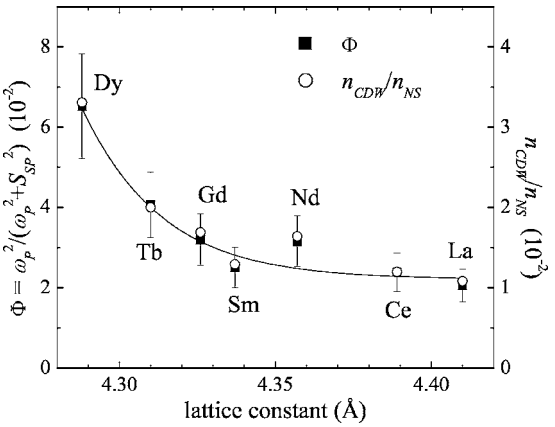

FIG. 4. Ratios $\Phi=\omega_P^2/(\omega_P^2+S_{SP}^2)$ (indicating the fraction of the ungapped FS) and n_{CDW}/n_{NS} as a function of the in-plane lattice constant (Ref. 12). The left and right scales differ by a factor of 2. The rare-earth atom for each compound is shown in the plot. The solid line is a guide to eyes.

of the Drude peak and the total spectral weight of the Drude term and the SP peak (Table I). Φ roughly measures, as previously shown in Ref. 22, the fraction of the ungapped FS area (i.e., those parts of FS which are not affected by the CDW state). Since the effective mass of the free carriers is different in CDW and NS, Φ does not simply reduce to n_{CDW}/n_{NS} and it is larger than the latter quantity by a factor given by $m_{NS}/m_{CDW}\sim 2$. Although the Φ values seem to significantly underestimate the fraction of the ungapped FS compared to the estimate evinced from ARPES data,[15–18] they at least qualitatively confirm that a large portion of FS is gapped. The difference between ARPES and optics, as far as the gapping of FS is concerned, may also be reconciled in part by taking into account the energy resolution of the ARPES data.[30] We now turn to the evolution of the CDW state across the rare-earth series. First of all, the reduction of ω_{SP} on decreasing a [Fig. 3(b)] may be considered as an indication for the diminishing impact of the CDW state, when going from La to Dy. Such a gap reduction is also consistent with the ARPES data,[19] showing a gap of about 400 meV in $CeTe_3$,[15,16] and a gap of 200 meV in $SmTe_3$.[17] In recent ARPES experiments[18] a reduction of the maximum gap value with decreasing a was also observed for several compounds of the RTe_3 series. It is important to remark that, differently from ARPES where the maximum gap value can be determined, our optical estimate provides a sort of averaged value for the CDW gap over the whole FS.

In Fig. 4, Φ (Table I) is plotted as a function of the lattice constant a.[12] The portion of the ungapped FS increases on decreasing a and has a more gradual and less scattered behavior than ω_P [Fig. 3(a)]. Since Φ corresponds to the ratio between spectral weights, it is less affected by possible uncertainties of the $\sigma_1(\omega)$ absolute value. In the same figure, the ratio n_{CDW}/n_{NS} between the carrier's densities in the CDW and NS (see Table I) is also plotted as a function of a. As discussed above, the two quantities have the same dependence on a and just differ in absolute value by a factor ~2 (Fig. 4), coming from the effective mass ratio. The increase of Φ with decreasing a is quite abrupt for rare earths beyond

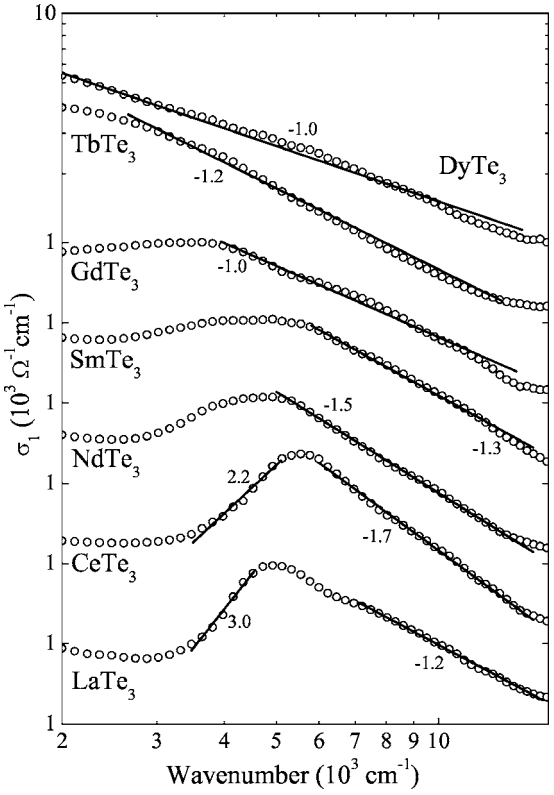

FIG. 5. $\sigma_1(\omega)$ of RTe_3 (R is La, Ce, Nd, Sm, Gd, Tb, and Dy) plotted on a bilogarithmic scale. The y-axis logarithmic scale is vertically shifted for the sake of clarity. The scale is the same for all samples and the scale offset is shown for each spectrum. The solid lines are power-law fits to the data (the exponents are given in the figure).

the Sm-containing compound, indicating the onset of a chemical pressure effect for $a\leq 4.34$ Å. On the other hand, the effective mass is almost constant across the rare-earth series so that the band-shape and the inertia of the free charge carriers are only subtly affected by the lattice compression. Therefore, this seems to rule out a large change in the bandwidth. Nevertheless, one cannot exclude *a priori* that a yet subtle narrowing of the bands with increasing lattice constant could lead to a better nesting and to differences in the amount of the nested FS.

In this context, it is then quite natural to assume that the reduction of ω_{SP} [Fig. 3(b)] on going from $LaTe_3$ to $DyTe_3$ could be ascribed to a suppression of the nesting condition, due to the changes in FS, because of the lattice compression. In this scenario, the increase of the ungapped portions of FS with decreasing a (Fig. 4) leads to an enhanced optical contribution due to the free charge carries. The strong decrease of ω_{SP} is consistent with the reduction of the perfectly-nested regions (where the CDW gap is close to its maximum value) in favor of the nonperfectly-nested regions (where the gap is close to zero).

Finally, a power-law $[\sigma_1(\omega)\sim\omega^{\eta}]$ behavior for the high-frequency tail of the SP peak is observed in all samples. This is shown in Fig. 5, where $\sigma_1(\omega)$ is plotted on bilogarithmic scale. The power-law behavior extends over a rather limited energy interval, which at most is one order of magnitude

wide for the Dy compound. Power-law scaling is indicative of quasi 1D behavior.[31,32] The observed exponents, although not precisely determined, give indications as to the mechanism behind CDW formation in these materials. In the following analysis we make the case that electron-electron interactions play a crucial role in the CDW formation in $R\mathrm{Te}_3$.

The traditionally invoked mechanism for CDW formation is the electron-phonon coupling. In that case there are three energy scales to be considered for optical absorption: the typical phonon frequency ω_0, the single-particle (or Peierls) gap Δ, and the frequency ω at which the measurement is done. As anticipated above, the advocated FS of the material[15] consists of two sheets of open FS's of a quasi 1D material (associated to the p_x and p_y orbitals, respectively). The measured vector for the CDW modulation is very close to the vector that corresponds to the nesting of the two sides of this quasi 1D FS. Attributing the one dimensionality to the fact that $R\mathrm{Te}_3$ have a nearly perfect nested quasi 1D FS is of particular relevance here, since the charge transfer integral (t_{perp}) along the transverse direction (i.e., describing the hopping between the p_x and p_y orbitals) is not small and is much larger than the temperature of the measurements. Indeed, $t_{perp} > T$ would normally lead to coherent transverse hopping, so that FS would have significant warping in the transverse direction and the material would not be 1D anymore. The warping of FS would loose its relevance only at $\omega > t_{perp}$. However, this is not the appropriate situation for $R\mathrm{Te}_3$, since $t_{perp}=0.37$ eV,[13,15] while the power-law behavior is observed for frequencies $\omega > 0.2$ eV. But if nesting is strong and occurs with a well-defined $\vec{q}$ vector, then the system still acts as a 1D system would essentially do. The 1D character, indicated by the high-frequency power-law behavior of $\sigma_1(\omega)$ (Fig. 5), may then persist even for $\omega \leqslant t_{perp}$, provided that one looks at phenomena involving the nesting wave vector.

In the case of a 1D material, one would obtain different exponents for the optical behavior above the Peierls gap depending on the hierarchy of the energy scales, pointed out above. If one is in the so-called adiabatic limit $\omega_0 \ll \Delta$ where the phonon frequency is quite small, then one can assimilate the potential created by the phonons to either a periodic (with wave vector $\vec{q}$) static deformation, if $\omega \ll \omega_0$, or to a quenched disorder varying in space, if $\omega \gg \omega_0$. In the first case the conductivity can easily be computed by looking at the scattering on the static periodic potential with a wave vector $\vec{q}$, the CDW modulation vector, using the techniques explained in Ref. 33. One finds that $\sigma_1(\omega) \propto \omega^{K_\rho - 4}$, where $K_\rho < 1$ is the Luttinger liquid parameter. $K_\rho = 1$ for a Fermi liquid or if interactions are weak and decreases with increasingly repulsive interactions. It is clear that such a result would not be compatible with the data, making it hard to have the standard adiabatic mechanism for the CDW formation. The other case, when the phonon potential is viewed by the electron as a quenched disorder, is also not quite compatible with the data. Indeed in that case one finds $\sigma_1(\omega) \propto \omega^{K_\rho - 3}$.[33] A weakly interacting system would thus give exponents of order -2 or slightly below, in somewhat closer but yet very unsatisfactory agreement with the data. It thus seems unlikely that the data are explained by the standard scattering over a distortion due to adiabatic phonons. The data would on the contrary be in reasonable agreement with the so-called antiadiabatic limit $(\Delta, \omega) \ll \omega_0$, in which one can integrate over the phonon field. The phonon fluctuations introduce then an effective interaction between the particles. This interaction corresponds to an umklapp scattering, which gives[6,33]

$$\sigma_1(\omega) \propto \omega^{4K_\rho - 5}. \tag{6}$$

This would lead to exponents η close or slightly smaller than -1, in much better agreement with the data. It is however extremely unlikely to be able to find phonons of such high frequency, since one would need $\omega_0 > 1$ eV. Consequently, phonons alone could not explain the observed optical data and power laws.

A much more probable source for such an umklapp scattering leading to Eq. (6) is the direct interaction between electrons. Such an interaction can directly produce an umklapp scattering, allowing the transfer of two particles from one sheet of the FS to the other and thus transferring $4\vec{q}$ to the lattice.[33] Note that the advocated wave vector[15] for the CDW modulation is indeed giving a value for $4\vec{q}$ close to a reciprocal lattice vector, and thus allowing such umklapp processes to be effective. An umklapp process leading to a power law behavior in $\sigma_1(\omega)$ and in other response functions was theoretically predicted for strict 1D systems within the Tomonaga-Luttinger-liquid scenario[6] and observed experimentally in the 1D Bechgaard salts with $\eta = -1.3$.[7,31,32] Furthermore, we identify in $\sigma_1(\omega)$ of the Ce and La compounds a low-frequency tail of the SP peak following a power-law behavior as well (Fig. 5). The resulting exponent ranges between 2.2 and 3, which again compares quite well with the value of 3 predicted for a 1D Mott insulator for which umklapp is the dominant source of scattering.[7]

Even though the exponents for the high-frequency power-law observed in our data do not show a defined trend across the rare-earth series, their values range between -1.7 and -1.0. This is in decent agreement with such a scenario where interactions and umklapp would be responsible for the observed behavior. This strongly suggests that interactions rather than a standard electron-phonon mechanism could play, in the rare-earth tri-telluride compounds a crucial role in the CDW formation as well. Of course more studies both theoretically and experimentally would be useful to ascertain the respective roles of the interactions and of electron-phonon coupling with respect to the CDW formation. Theoretically, a more careful treatment of the effects of the transverse warping of FS would be clearly needed, not only for the high-energy behavior but even more for the low-frequency part of the optical conductivity, much below the single-particle peak.

IV. CONCLUSIONS

In summary, we reported on the first optical measurements of seven different rare-earth tri-telluride compounds. Our data allow for a detailed analysis of both the Drude

contribution, ascribed to the free charge carriers resulting from the presence of ungapped regions of FS, and the SP peak, due to carriers' excitation across the CDW gap. On decreasing the lattice constant, a slight enhancement of the metallic contribution and a simultaneous reduction of the CDW gap are observed. We propose that this effect might be due to a quenching of the nesting condition driven by a modification of FS because of the lattice compression. We also observe power-law behaviors in $\sigma_1(\omega)$, typical of a Tomonaga-Luttinger-liquid system, which emphasize a non-negligible contribution of 1D correlation effects in the physics of these 2D compounds. This also anticipates that interactions and umklapp processes could play a significant role in the CDW formation in these compounds.

ACKNOWLEDGMENTS

The authors wish to thank J. Müller for technical help, and V. Brouet and M. Lavagnini for fruitful discussions. One of us (A.S.) wishes to acknowledge the scholarship of the Della Riccia Foundation. This work has been supported by the Swiss National Foundation for Scientific Research within the NCCR MaNEP pool. This work is also supported by the Department of Energy, Office of Basic Energy Sciences under Contract No. DE-AC02-76SF00515.

[1] *Strong Interactions in Low Dimensions*, edited by D. Baeriswyl and L. Degiorgi (Kluwer Academic, Dordrecht, 2004).
[2] G. Grüner, *Density Waves in Solids* (Addison-Wesley, Reading, MA, 1994).
[3] R. Peierls, *Quantum Theory of Solids* (Clarendon Press, Oxford, 1955).
[4] D. Jérome and H. J. Schulz, Adv. Phys. **31**, 299 (1982).
[5] J. Voit, Rep. Prog. Phys. **58**, 977 (1995).
[6] T. Giamarchi, Physica B **230-232**, 975 (1997).
[7] V. Vescoli, F. Zwick, W. Henderson, L. Degiorgi, M. Grioni, G. Gruner, and L. K. Montgomery, Eur. Phys. J. B **13**, 503 (2000).
[8] E. DiMasi, B. Foran, M. C. Aronson, and S. Lee, Chem. Mater. **6**, 1867 (1994).
[9] E. DiMasi, M. C. Aronson, J. F. Mansfield, B. Foran, and S. Lee, Phys. Rev. B **52**, 14516 (1995).
[10] B. K. Norling and H. Steinfink, Inorg. Chem. **5**, 1488 (1966).
[11] The *Cmcm* space group is orthorhombic. However, the in-plane lattice constants *a* and *c* differ by approximately 0.1% (in the standard space group setting the *b* axis is perpendicular to the Te planes). For simplicity, in our subsequent analysis we treat the material as essentially tetragonal, characterized by an in-plane lattice constant *a*.
[12] P. Villars and L. D. Calvert, *Pearson's Handbook of Crystallographic Data for Intermetallic Phases* (American Society for Metals, Metals Park, OH, 1991).
[13] A. Kikuchi, J. Phys. Soc. Jpn. **67**, 1308 (1998).
[14] J. Laverock, S. B. Dugdale, Zs. Major, M. A. Alam, N. Ru, I. R. Fisher, G. Santi, and E. Bruno, Phys. Rev. B **71**, 085114 (2005).
[15] V. Brouet, W. L. Yang, X. J. Zhou, Z. Hussain, N. Ru, K. Y. Shin, I. R. Fisher, and Z. X. Shen, Phys. Rev. Lett. **93**, 126405 (2004).
[16] H. Komoda, T. Sato, S. Souma, T. Takahashi, Y. Ito, and K. Suzuki, Phys. Rev. B **70**, 195101 (2004).
[17] G.-H. Gweon, J. D. Denlinger, J. A. Clack, J. W. Allen, C. G. Olson, E. D. DiMasi, M. C. Aronson, B. Foran, and S. Lee, Phys. Rev. Lett. **81**, 886 (1998).
[18] V. Brouet, W. L. Yang, X. J. Zhou, Z. Hussain, N. Ru, I. R. Fisher, and Z. X. Shen (unpublished).
[19] The gap values determined from the ARPES experiments are always referred with respect to the Fermi energy. Assuming the Fermi energy in the middle of the gap, means that the optically determined gap is about twice as large as the ARPES one.
[20] V. Vescoli, L. Degiorgi, H. Berger, and L. Forró, Phys. Rev. Lett. **81**, 453 (1998).
[21] S. V. Dordevic, D. N. Basov, R. C. Dynes, and E. Bucher, Phys. Rev. B **64**, 161103(R) (2001).
[22] A. Perucchi, L. Degiorgi, and R. E. Thorne, Phys. Rev. B **69**, 195114 (2004).
[23] A. Perucchi, C. Søndergaard, S. Mitrovic, M. Grioni, N. Barisic, H. Berger, L. Forró, and L. Degiorgi, Eur. Phys. J. B **39**, 433 (2004).
[24] P. A. Lee, T. W. Rice, and P. M. Anderson, Solid State Commun. **14**, 703 (1974).
[25] N. Ru and I. R. Fisher, Phys. Rev. B **73**, 033101 (2006).
[26] F. Wooten, *Optical Properties of Solids* (Academic Press, New York, 1972).
[27] M. Dressel and G. Grüner, *Electrodynamics of Solids* (Cambridge University Press, Cambridge, England, 2002).
[28] Y. Iyeiri, T. Okumura, C. Michioka, and K. Suzuki, Phys. Rev. B **67**, 144417 (2003).
[29] K. Y. Shin, V. Brouet, N. Ru, Z. X. Shen, and I. R. Fisher, Phys. Rev. B **72**, 085132 (2005).
[30] Fermi surface, reconstructed from ARPES data, corresponds to integrated signals up to an energy window around the Fermi energy. Therefore, the gapping of the Fermi surface will only extend over regions corresponding to gap values larger than the experimental resolution, while the real gap extends further around the Fermi surface than its ARPES mapping appears to show.
[31] V. Vescoli, L. Degiorgi, W. Henderson, G. Grüner, K. P. Starkey, and L. K. Montgomery, Science **281**, 1181 (1998).
[32] A. Schwartz, M. Dressel, G. Grüner, V. Vescoli, L. Degiorgi, and T. Giamarchi, Phys. Rev. B **58**, 1261 (1998).
[33] T. Giamarchi, *Quantum Physics in One Dimension* (Oxford University Press, Oxford, 2004).